

THE ZEEMAN EFFECT IN ASTROPHYSICAL WATER MASERS AND THE OBSERVATION OF STRONG MAGNETIC FIELDS IN REGIONS OF STAR FORMATION

GERALD E. NEDOLUHA¹

Code 4210, Naval Research Laboratory, Washington, DC 20375-5000

AND

WILLIAM D. WATSON²

Departments of Physics and Astronomy, University of Illinois at Urbana-Champaign, Urbana, IL 61801

Received 1991 May 8; accepted 1991 July 15

ABSTRACT

The transfer equations for the polarized radiation of astrophysical, 22 GHz water masers are solved in the presence of a magnetic field which causes a Zeeman splitting that is much smaller than the spectral line breadth. We focus upon the relationship between the recently detected circular polarization in this maser radiation and the strength of the magnetic field. In initial assessments, others have found that the observed polarization is indicative of the strongest magnetic fields yet detected in regions of star formation (≈ 50 mG).

In these estimates for the magnetic field, important ways in which the transfer of the 22 GHz maser radiation differs from the transfer of nonmaser radiation due to a single transition have not been considered. These include the narrowing and rebroadening of the spectral line with increasing optical depth, the merging of hyperfine components, deviations of the molecular velocities from a Maxwellian distribution, unequal populations of the magnetic substates, the influence of cross-relaxation, and the generation of circularly polarized radiation due to changes in direction of the linear polarization.

Major uncertainties in the inferred strengths of the magnetic fields due to these considerations tend to occur mostly when the flux of maser radiation is high and the maser is saturated. The observed spectral line breadths are found to be good indicators of whether the radiative flux is high enough that such effects are significant. For example, when the breadth is smaller than about 0.8 km s^{-1} (FWHM), we calculate that the uncertainty is less than a factor of about 2. The accuracy is improved significantly when the angle between the line of sight and the direction of the magnetic field does not exceed $\sim 45^\circ$. Our “best values” for the strengths of the inferred magnetic fields are about $\frac{2}{3}$ of those obtained previously. For the maser fluxes and for the magnetic field strengths believed to be relevant, the Zeeman frequency is much greater than the rate for stimulated emission. The calculations here are performed with approximations appropriate for this regime.

Uncertainty in the strength of the magnetic field due to lack of knowledge about which hyperfine transition is the source of the 22 GHz masers is removed. The 22 GHz maser feature is found to be the result of a merger of the three strongest hyperfine components. The merger itself introduces little uncertainty. This overlapping of the hyperfine components, by itself, causes the profile for the net circular polarization (i.e., the Stokes V parameter) to be quite asymmetric. One sense of the circular polarization tends to dominate.

Subject headings: atomic processes — ISM: magnetic fields — masers — polarization — stars: formation

1. INTRODUCTION

Fiebig & Güsten (1989, hereafter FG) have reported the detection of weak circular polarization (about 10^{-3} fractionally) in the spectra of 22 GHz water masers in regions of star formation. The polarization is believed to be a result of the Zeeman effect in which the splittings due to the magnetic field are much smaller than the spectral line breadth. A straightforward analysis similar to that used for nonmasing spectral lines at radio frequencies yields, for the typical strength of the component of the magnetic field parallel to the line of sight, $B \cos \theta = 50, 80,$ or 670 mG depending upon which of the three strongest hyperfine transitions (7–6, 6–5, or 5–4) is assumed to be the masing transition. Such magnetic fields are reasonable. Magnetic field strengths of 1–10 mG are indicated from observations of OH masers in regions of star formation. Stronger magnetic fields in the water masers are plausible since they probably are in gas that is more dense by factors of 10–1000 than that of the OH masers. The Zeeman features of the OH masers in these regions are well separated, and their interpretation is not susceptible to the same types of uncertainties as for the H_2O masers. Magnetic fields are believed to play an important role in the formation of stars and in the gas dynamics of star-forming regions. Their detection at the highest gas densities and closest to the centers of star formation is thus of particular significance. The magnetic field strengths inferred from the observations of 22 GHz water masers are the strongest yet detected in regions of star formation.

Inferences about the strengths of the magnetic field B from the observations of water masers have been based upon the relationship (FG)

$$\Delta V \Delta v / I_0 \equiv (V_{\max} - V_{\min}) \Delta v / I_0 = 2 \mathcal{A} B \cos \theta, \quad (1)$$

¹ National Research Council/NRL Cooperative Research Associate, Washington, D.C.

² Postal address: Department of Physics, University of Illinois at Urbana-Champaign, 1110 West Green Street, Urbana, IL 61801.

for Zeeman shifts of the spectral lines that are much smaller than the spectral line breadth. Here V_{\max} and V_{\min} are maximum and minimum values of Stokes V parameter across the spectral line ($V =$ left circularly polarized intensity minus right circularly polarized intensity; note that the sign of V here is opposite to that of FG). In equation (1), $\Delta\nu$ is the width of the spectral line (FWHM) in km s^{-1} , I_0 is the intensity at line center, θ is the angle between the direction of the magnetic field and the direction of propagation of the radiation, and \mathcal{A} is a constant that depends upon the particular molecular transition ($\mathcal{A} = 13.4, 8.3,$ and 1.0×10^{-3} , respectively, for the $F = 7-6, 6-5,$ and $5-4$ hyperfine components of the 22 GHz transition). An expression of the form of equation (1) is commonly used for interpreting the circular polarization of nonmasing spectral lines. It has been obtained for the 22 GHz masers by treating the spectral line in a manner similar to that for nonmasing transitions. This ignores a number of seemingly important aspects of the radiative transfer of masers. For a maser, the spectral line first narrows as a function of optical depth to about one-fifth of its original breadth and then rebroadens after the maser becomes radiatively saturated (Litvak 1970). In saturated masers, the velocities of the molecules in the masing states can deviate from a Maxwellian distribution, and the populations of the magnetic substrates of an energy level can become unequal. Cross-relaxation due to trapped infrared radiation is expected to be rapid. This process influences the distributions of molecular velocities and the population of hyperfine states and magnetic substrates. We have, in addition, recently shown that circularly polarized radiation is generated as a result of the change in direction of the linear polarization when the stimulated emission rate approaches the Zeeman frequency (Nedoluha & Watson 1990b). In certain assessments of the 22 GHz masers, it has been concluded that they are highly saturated with radiative fluxes that are larger by factors of 100 than the minimum flux for saturation (e.g., Reid & Moran 1981). The rate for stimulated emission would then be about 100 s^{-1} and similar to the indicated Zeeman frequencies. In this case, the above effects should certainly be important and the radiative transfer would be expected to be quite different from that of nonmasing transitions. Finally, we have shown that the 22 GHz spectral line actually is composed of all three of the strongest hyperfine transitions under plausible physical conditions (Nedoluha & Watson 1991).

In § 2 we describe the basic physical processes for the transport of polarized maser radiation in the presence of a magnetic field that causes Zeeman splittings which are much smaller than the spectral line breadth. The results of the numerical solution of the equations of radiative transfer and the associated rate equations for the molecular populations are presented in § 3. We focus on examining the usefulness of equation (1) for the 22 GHz maser radiation. Our conclusions about the reliability of the 22 GHz maser radiation as a diagnostic for strong magnetic fields in star-forming and other regions of the interstellar gas are summarized in § 4. We find that the observed spectral line breadth is a useful indicator for the possible deviations from equation (1).

2. BASIC EQUATIONS

2.1. Without Explicitly Including Cross-Relaxation

We calculate the intensity, linear polarization, and circular polarization (the Stokes $I, Q,$ and V parameters, respectively) due to the combined effects of the three strongest hyperfine components. The separations are 0.45 and 0.58 km s^{-1} between the $F = 7-6, 6-5,$ and $5-4$ components, and the relative line strengths are $0.385, 0.324,$ and $0.273,$ respectively. We have verified in previous calculations that only these three components make a significant contribution (Deguchi & Watson 1986; Nedoluha & Watson 1991). The calculations below are performed for the regime in which the Zeeman frequency $g\Omega$ is much greater than the rate for stimulated emission $R,$ the decay rate Γ for the molecular excitations, and the rate Γ_p for cross-relaxation. The exact relevance of this regime of parameters to the observations will be discussed in §§ 3 and 4, as well as the relaxation of the molecular states. In this regime, the calculations are greatly simplified because the off-diagonal elements are negligible in the quantum mechanical density matrix that describes the molecular states. Ordinary rate equations for the populations of the magnetic substrates are then adequate. These can be obtained directly from the more general forms of the equations given by Deguchi & Watson (1990; see their eqs. [A39] and [A40]). For the number density of water molecules $n(F, a, v)$ as a function of molecular velocity v parallel to the direction of propagation of the maser radiation, and in the magnetic substate a of the hyperfine state F of the upper (6_{16}) rotational state,

$$\begin{aligned}
 0 = & \lambda_F(v) - \Gamma n(F, a, v) - (2\pi/c\hbar^2)\Delta\Omega \sum_b \left\{ [n(F, a, v) - n(F', b, v)] \int d\omega \gamma_{ab}^F [I(\omega)(\langle Fa|d_+|F'b\rangle^* \langle Fa|d_+|F'b\rangle \right. \\
 & + \langle Fa|d_-|F'b\rangle^* \langle Fa|d_-|F'b\rangle) - Q(\omega)(\langle Fa|d_+|F'b\rangle^* \langle Fa|d_-|F'b\rangle + \langle Fa|d_-|F'b\rangle^* \langle Fa|d_+|F'b\rangle) \\
 & \left. + V(\omega)(\langle Fa|d_+|F'b\rangle^* \langle Fa|d_+|F'b\rangle - \langle Fa|d_-|F'b\rangle^* \langle Fa|d_-|F'b\rangle)] \right\} \quad (2)
 \end{aligned}$$

in the usual approximation of steady state. The pumping rate λ_F has a Maxwellian velocity dependence and is the same for all magnetic substrates (isotropic pumping) and all hyperfine states of the 6_{16} energy level, Γ is the decay rate for the molecular excitation, and the integral is over the angular frequency ω of the maser radiation. There are similar rate equations for the number of densities $n(F', b, v)$ in the magnetic substrates b of the F' hyperfine states of the lower (5_{23}) rotational state. An integration over angles is not necessary in equation (2) because we make the usual approximation of nearly one-dimensional propagation for the maser radiation. The angular integration is thus replaced by the solid angle $\Delta\Omega$ for the beaming of the maser radiation. Also

$$\gamma_{ab}^F = \frac{\Gamma}{\Gamma^2 + [\omega_{ab}^F - \omega(1 - v/c)]^2}, \quad (3)$$

where ω_{ab}^F is the angular frequency of the radiation between the magnetic substate a of the hyperfine state F and the substate b of the hyperfine state $F' = F - 1$. With an angle θ between the direction of propagation of the maser radiation and the direction of the

magnetic field, the matrix elements are

$$\langle Fa|d_+|F'b\rangle = \langle Fa|d_{M=1}|F'b\rangle(1 + \cos \theta)/2 + i\langle Fa|d_{M=0}|F'b\rangle \sin \theta/\sqrt{2} - \langle Fa|d_{M=-1}|F'b\rangle(1 - \cos \theta)/2 \quad (4)$$

and

$$\langle Fa|d_-|F'b\rangle = -\langle Fa|d_{M=1}|F'b\rangle(1 - \cos \theta)/2 + i\langle Fa|d_{M=0}|F'b\rangle \sin \theta/\sqrt{2} + \langle Fa|d_{M=-1}|F'b\rangle(1 + \cos \theta)/2 \quad (5)$$

in terms of the dipole matrix elements in the coordinate system with its z-axis parallel to the magnetic field,

$$|\langle Fa|d_M|F'b\rangle|^2 = \frac{hc^3}{\omega^3} \frac{3}{8\pi} \mathbf{A}_{F,F-1} [C(F-1, 1, b, M|Fa)]^2. \quad (6)$$

In equation (6), $C(F-1, 1, b, M|F, a)$ is a Clebsch-Gordon coefficient (e.g., Messiah 1962; also Deguchi & Watson 1990) and

$$\mathbf{A}_{F,F-1} = 1.858 \times 10^{-9} [39 LS_{F,F-1}/(2F+1)] s^{-1}, \quad (7)$$

where $LS_{F,F-1}$ is the fractional line strength (0.385, 0.324, or 0.273) of the hyperfine F to $F-1$ transition (e.g., Townes & Schawlow 1975; also Deguchi & Watson 1986).

The equations of radiative transfer for the Stokes parameters per unit angular frequency $I(\omega)$, $Q(\omega)$ and $V(\omega)$ which represent the total intensity, linearly polarized intensity, and circularly polarized intensity, respectively, are (Deguchi & Watson 1990)

$$\frac{dI(\omega)}{ds} = (A_\omega^{76} + A_\omega^{65} + A_\omega^{54})I(\omega) + (B_\omega^{76} + B_\omega^{65} + B_\omega^{54})Q(\omega) + (C_\omega^{76} + C_\omega^{65} + C_\omega^{54})V(\omega), \quad (8)$$

$$\frac{dQ(\omega)}{ds} = (A_\omega^{76} + A_\omega^{65} + A_\omega^{54})Q(\omega) + (B_\omega^{76} + B_\omega^{65} + B_\omega^{54})I(\omega), \quad (9)$$

and

$$\frac{dV(\omega)}{ds} = (A_\omega^{76} + A_\omega^{65} + A_\omega^{54})V(\omega) + (C_\omega^{76} + C_\omega^{65} + C_\omega^{54})I(\omega). \quad (10)$$

Here, s is the distance measured along the direction of propagation and the coefficients are determined from the populations of the magnetic substrates,

$$A_\omega^{FF'} = \frac{2\pi\omega}{c\hbar} \sum_{a,b} \int dv \{ [n(F, a, v) - n(F', b, v)] \gamma_{ab} (\langle Fa|d_+|F'b\rangle^* \langle Fa|d_+|F'b\rangle + \langle Fa|d_-|F'b\rangle^* \langle Fa|d_-|F'b\rangle) \}, \quad (11)$$

$$B_\omega^{FF'} = -\frac{2\pi\omega}{c\hbar} \sum_{a,b} \int dv \{ [n(F, a, v) - n(F', b, v)] \gamma_{ab} (\langle Fa|d_+|F'b\rangle^* \langle Fa|d_-|F'b\rangle + \langle Fa|d_-|F'b\rangle^* \langle Fa|d_+|F'b\rangle) \}, \quad (12)$$

and

$$C_\omega^{FF'} = \frac{2\pi\omega}{c\hbar} \sum_{a,b} \int dv \{ [n(F, a, v) - n(F', b, v)] \gamma_{ab} (\langle Fa|d_+|F'b\rangle^* \langle Fa|d_+|F'b\rangle - \langle Fa|d_-|F'b\rangle^* \langle Fa|d_-|F'b\rangle) \}. \quad (13)$$

The integrals over velocity and angular frequency can be evaluated to sufficient accuracy by recognizing that γ_{ab}^F is strongly peaked so that

$$\int dv \gamma_{ab}^F n(F, a, v) \simeq n[F, a, c(\omega - \omega_{ab}^F)/\omega] \int dv \gamma^{ab} \simeq \pi c n[F, a, c(\omega - \omega_{ab}^F)/\omega] / \omega \quad (14)$$

and

$$\int d\omega \gamma_{ab}^F I(\omega) \simeq I[\omega_{ab}^F/(1-v/c)] \int d\omega \gamma_{ab}^F \simeq \pi I[\omega_{ab}^F/(1-v/c)]. \quad (15)$$

We numerically evaluate the equations of radiative transfer at enough frequencies ω_j (typically 100) to characterize the spectral line profile. This requires that the populations be evaluated at the related velocities; i.e., for populations $n(F, a, v)$ and $n(F' = F-1, b, v)$ at the velocities given by

$$\omega_{00}^F - \omega_j(1 - v_j^F/c) = 0. \quad (16)$$

Here ω_{00}^F is angular frequency of the radiation between the hyperfine F and $F' = F-1$ states in the absence of a magnetic field. Equation (16) defines v_j^F . The populations that are required, for example, to apply equation (14) can then be found to sufficient accuracy in terms of the populations and their derivatives at v_j^F ; e.g.,

$$n[F, a, c(\omega_j - \omega_{ab}^F)/\omega_j] \simeq n(F, a, v_j^F) - \left. \frac{\partial n(F, a, v)}{\partial v} \right|_{v_j^F} \cdot \frac{c}{\omega_j} \left(M_a \frac{g\Omega^F}{2} - M_b \frac{g\Omega^{F'}}{2} \right), \quad (17)$$

where M_a and M_b are the quantum numbers of the magnetic substates a and b . Similarly,

$$I[\omega_{ab}^F/(1 - v_j^F/c)] \simeq I(\omega_j) + \left. \frac{\partial I(\omega)}{\partial \omega} \right|_{\omega=\omega_j} \cdot \left(M_a \frac{g\Omega^F}{2} - M_b \frac{g\Omega^{F'}}{2} \right). \quad (18)$$

The derivatives are evaluated in terms of the populations and intensities at $(j + 1)$ and $(j - 1)$.

The shifts in energy due to the magnetic field B for the energy levels of water characterized by the quantum numbers (J, F, I) and magnetic substate M_F are (e.g., Gordy & Cook 1970; also FG)

$$\Delta E = -(\alpha_J g_J + \alpha_I g_I) \mu_N M_F B \equiv M_F \hbar \frac{g\Omega^F}{2}, \quad (19)$$

where

$$\alpha_J = [J(J + 1) + F(F + 1) - I(I + 1)]/2F(F + 1) \quad (20)$$

and

$$\alpha_I = [F(F + 1) + I(I + 1) - J(J + 1)]/2F(F + 1) \quad (21)$$

(eqs. [19]–[21] are also valid when F and J are replaced by F' and J'). Here, μ_N is the nuclear magneton, $g_I = 5.585$, $g_6 = 0.6565$ and $g_5 = 0.6959$ (Kukolich 1969). Since $g\Omega^F \neq g\Omega^{F'}$, the Zeeman shifts of the various spectral lines of a specified ΔM (e.g., $\Delta M = +1$) are not equal but spread over a range of frequencies that is comparable with the average difference in frequency between the $\Delta M = +1$ and $\Delta M = -1$ groups of spectral lines. The foregoing gives for the 6_{16} state, (in radians s^{-1}), $g\Omega^7/2 = 6510$, $g\Omega^6/2 = 3710$, and $g\Omega^5/2 = -790$ whereas for the 5_{23} state, $g\Omega^6/2 = 7240$, $g\Omega^5/2 = 4120$, and $g\Omega^4/2 = -1340$.

2.2. Cross-Relaxation

In equation (2), the effect of “cross-relaxation” is not explicitly included. Trapped infrared radiation involving the maser states tends to randomize the molecular velocities of the populations of the masing states (Goldreich & Kwan 1974). It also tends to randomize the populations of the magnetic substates and the populations of the hyperfine states (Goldreich, Keeley, & Kwan 1973). The rates at which these three types of relaxation occur are not exactly the same but should be similar. They occur with essentially every emission or absorption of an infrared photon by a masing state. The relevant rate is roughly the sum of the inverse lifetimes of the states for emission of infrared radiation—a rate that is insensitive to exact physical conditions of the masing gas. In contrast, the emission of an infrared photon by a masing state contributes to the decay of molecular excitation Γ only when the photon escapes from the gas or is otherwise eliminated. These infrared transitions ordinarily are expected to have large optical depths in the water masers. Most such infrared photons are then reabsorbed and simply excite another water molecule. Cross-relaxation is thus expected to be effective with a rate Γ_v that is considerably larger than the decay rate Γ . A detailed calculation of the relaxation of the molecular velocities gives $\Gamma_v = 2 s^{-1}$ for this rate at 400 K (Anderson & Watson 1991) and is in excellent agreement with the estimate of $1 s^{-1}$ at the same temperature by Goldreich & Kwan (1974). “Elastic” collisions between the masing water molecules and hydrogen molecules can, in principle, also cause the relaxation of the molecular velocities (Nedoluha & Watson 1988). However, the rate for this relaxation process is slower than that for trapped infrared radiation in the 22 GHz water masers and is unimportant (Anderson & Watson 1991).

The effect of relaxation is to drive the velocities toward a Maxwellian distribution and to drive the populations of the magnetic substates of a rotational energy level (i.e., the 6_{16} or the 5_{23}) toward equality. A reasonable way to approximate the effects of trapped radiation is then to assume that at every reabsorption of a trapped infrared photon, the newly excited molecule has a velocity that is randomly chosen from within a Maxwellian distribution and a magnetic substate that is chosen at random from the substates of the rotational energy level of the original, excited molecule. The likelihood of a particular hyperfine state is then proportional to its degeneracy. The foregoing idealization has the desirable feature that it yields the correct solutions in the limit of very large (as well as small) rates for cross-relaxation. Equation (2) would thus be modified by subtracting a term $\Gamma_v n(F, a, v)$ and by adding

$$\Gamma_v \phi(v) \sum_{F,a} \int dv n(F, a, v) / \sum_F (2F + 1), \quad (22)$$

where $\phi(v)$ is a normalized Maxwellian velocity distribution at the kinetic temperature of the gas (e.g., Nedoluha & Watson 1991). The rate equation for $n(F', b, v)$ would be modified in a similar manner. We now show that for the purposes here, introducing this cross-relaxation is equivalent to replacing Γ by $(\Gamma + \Gamma_v)$ in the equations of § 2.1. That is, whereas the solutions for the spectral line breadths and fractional polarization from the equations of § 2.1 scale with (flux/Γ) or $(I \Delta\Omega/\Gamma)$, they now scale with $[\text{flux}/(\Gamma + \Gamma_v)]$ or $[I \Delta\Omega/(\Gamma + \Gamma_v)]$.

First, from equation (2) modified with these terms for cross-relaxation together with the analogous rate equations for $n(F', b, v)$, generate linear equations in the population differences

$$\begin{aligned} 0 = & [\lambda_F(v) - \lambda_{F'}(v)] - (\Gamma + \Gamma_v)[n(F, a, v) - n(F', b, v)] \\ & - (2\pi/c\hbar^2) \sum_{b''} [n(F, a, v) - n(F', b'', v)] \int d\omega \gamma_{ab''} \{a, b''\} - (2\pi/c\hbar^2) \sum_{a''} [n(F, a'', v) - n(F', b, v)] \int d\omega \gamma_{a''b} \{a'', b\} \\ & + \Gamma_v \phi(v) \left[\left(\sum_F 2F + 1 \right)^{-1} \sum_{F,a'} \int dv n(F, a', v) - \left(\sum_{F'} 2F' + 1 \right)^{-1} \sum_{F',b'} \int dv n(F', b', v) \right], \quad (23) \end{aligned}$$

where

$$\begin{aligned} \{a, b\} = & I(\omega)\Delta\Omega(\langle Fa|d_+|F'b\rangle^*\langle Fa|d_+|F'b\rangle + \langle Fa|d_-|F'b\rangle^*\langle Fa|d_-|F'b\rangle) - Q(\omega)\Delta\Omega(\langle Fa|d_+|F'b\rangle^*\langle Fa|d_-|F'b\rangle \\ & + \langle Fa|d_-|F'b\rangle^*\langle Fa|d_+|F'b\rangle) + V(\omega)\Delta\Omega(\langle Fa|d_+|F'b\rangle^*\langle Fa|d_+|F'b\rangle - \langle Fa|d_-|F'b\rangle^*\langle Fa|d_-|F'b\rangle) \end{aligned} \quad (24)$$

with a' , a'' , b' , b'' substituted appropriately to obtain other expressions for the curly brackets as indicated. Separate out the Maxwellian velocity dependence in the pumping rate and express

$$\lambda_F(v) - \lambda_{F'}(v) = \phi(v)\Delta\Lambda. \quad (25)$$

Divide equation (23) by equation (25). Subtract the result from a second similar equation, but at a different velocity v' and with different substates a' and b' to obtain

$$\begin{aligned} 0 = & \left[\frac{n(F, a, v) - n(F', b, v)}{\phi(v)} \right] - \left[\frac{n(F_1, a', v') - n(F'_1, b', v')}{\phi(v')} \right] + (2\pi/c\hbar^2) \sum_{b''} \left[\frac{n(F, a, v) - n(F', b'', v)}{\phi(v)} \right] \int d\omega\gamma_{ab''} \frac{\{a, b''\}}{\Gamma + \Gamma_v} \\ & + (2\pi/c\hbar^2) \sum_{a''} \left[\frac{n(F, a'', v) - n(F', b, v)}{\phi(v)} \right] \int d\omega\gamma_{a''b} \frac{\{a'', b\}}{\Gamma + \Gamma_v} - (2\pi/c\hbar^2) \sum_{b''} \left[\frac{n(F_1, a', v') - n(F'_1, b'', v')}{\phi(v')} \right] \int d\omega\gamma_{a''b''} \frac{\{a', b''\}}{\Gamma + \Gamma_v} \\ & - (2\pi/c\hbar^2) \sum_{a''} \left[\frac{n(F_1, a'', v') - n(F'_1, b', v')}{\phi(v')} \right] \int d\omega\gamma_{a''b'} \frac{\{a'', b'\}}{\Gamma + \Gamma_v}. \end{aligned} \quad (26)$$

Equation (26) can be viewed as a large, homogeneous set of linear algebraic equations with the population differences divided by $\phi(v)$ as the unknowns. There can be as many choices of velocity as are needed to define molecular velocity distribution. This set of equations can be solved to yield the ratios of these population differences to a single population difference at a single velocity. That is, a solution can be found for

$$\frac{[n(F_1, a', v') - n(F'_1, b', v')]/\phi(v')}{[n(F, a, v) - n(F', b, v)]/\phi(v)}, \frac{[n(F_2, a'', v'') - n(F'_2, b'', v'')]/\phi(v'')}{[n(F, a, v) - n(F', b, v)]/\phi(v)}, \text{ etc.} \quad (27)$$

which depends upon the intensities only through the quantities $[I(\omega)\Delta\Omega/(\Gamma + \Gamma_v)]$, $[Q(\omega)\Delta\Omega/(\Gamma + \Gamma_v)]$ and $[V(\omega)\Delta\Omega/(\Gamma + \Gamma_v)]$. Equation (26) differs from what would be obtained in the absence of cross-relaxation only in the replacement of Γ by $(\Gamma + \Gamma_v)$. Hence the solutions in equation (27) that are found at intensities I , Q , and V in the absence of cross-relaxation will be valid at intensities $(I, Q, V) \times (\Gamma + \Gamma_v)/\Gamma$ when cross-relaxation is included.

We now show that the quantities of interest here—the fractional polarizations and the spectral line profile as represented by $[V(\omega)/I_0]$, $[Q(\omega)/I_0]$, and $[I(\omega)/I_0]$, where I_0 is the peak intensity—are functions only of $I_0\Delta\Omega/(\Gamma + \Gamma_v)$. Rearranging equations (8)–(10) yields

$$\frac{d[V(\omega)/I_0]}{d[I_0\Delta\Omega/(\Gamma + \Gamma_v)]} = \frac{1}{[I_0\Delta\Omega/(\Gamma + \Gamma_v)]} \left\{ \frac{(A_\omega/A_0)[V(\omega)/I_0] + (C_\omega/A_0)[I(\omega)/I_0]}{1 + (B_0/A_0)(Q_0/I_0) + (C_0/A_0)(V_0/I_0)} - \frac{V(\omega)}{I_0} \right\}, \quad (28)$$

$$\frac{d[Q(\omega)/I_0]}{d[I_0\Delta\Omega/(\Gamma + \Gamma_v)]} = \dots, \quad (29)$$

and

$$\frac{d[I(\omega)/I_0]}{d[I_0\Delta\Omega/(\Gamma + \Gamma_v)]} = \frac{1}{[I_0\Delta\Omega/(\Gamma + \Gamma_v)]} \left\{ \frac{(A_\omega/A_0)[I(\omega)/I_0] + (B_\omega/A_0)[Q(\omega)/I_0] + (C_\omega/A_0)[V(\omega)/I_0]}{1 + (B_0/A_0)(Q_0/I_0) + (C_0/A_0)(V_0/I_0)} - \frac{I(\omega)/I_0}{I_0\Delta\Omega/(\Gamma + \Gamma_v)} \right\}. \quad (30)$$

A_ω , B_ω , C_ω , A_0 , B_0 , and C_0 are linear in the $[n(F, a', v) - n(F', b', v)]$ and the ratios of all these to the chosen $[n(F, a, v) - n(F', b, v)]$ in equation (27) are functions only of the $I(\omega)\Delta\Omega/(\Gamma + \Gamma_v)$. The chosen $[n(F, a, v) - n(F', b, v)]$ then simply cancels out in the ratios (A_ω/A_0) , (C_ω/A_0) , etc. These terms are thus functions only of $I(\omega)\Delta\Omega/(\Gamma + \Gamma_v)$, $Q(\omega)\Delta\Omega/(\Gamma + \Gamma_v)$ and $V(\omega)\Delta\Omega/(\Gamma + \Gamma_v)$. Since the initial values of $Q(\omega)$ and $V(\omega)$ are zero, $Q(\omega)/I_0$ and $V(\omega)/I_0$ are also functions only of $I_0\Delta\Omega/(\Gamma + \Gamma_v)$ from equations (28)–(30). The solution of the entire calculation for $[V(\omega)/I_0]$, $[Q(\omega)/I_0]$, and $[I(\omega)/I_0]$ can then be expressed as a function of $I_0\Delta\Omega/(\Gamma + \Gamma_v)$ alone!

In summary, we can solve the equations of § 2.1 with Γ_v explicitly included and recognize that the solution can be scaled with $I_0\Delta\Omega/(\Gamma + \Gamma_v)$. That is, the effects of cross-relaxation on the spectral line profiles and fractional polarizations for a maser with a peak intensity I_0 are given exactly by these quantities computed in the absence of cross-relaxation but with a peak intensity $I_0 = I_0'\Gamma/(\Gamma + \Gamma_v)$. We have previously shown this to be valid for the spectral line profile [i.e., for $I(\omega)/I_0$] by explicit computation (Nedoluha & Watson 1991).

3. RESULTS OF CALCULATIONS

The foregoing equations are solved numerically in the usual approximation of one-dimensional propagation for the maser radiation. One-dimensional propagation is considered to be a good approximation because of the strong propensity for the maser rays that have paths with the greater amplifications to dominate (e.g., Alcock & Ross 1985). Evidence from the interpretation of the observations of the 22 GHz water masers also supports the premise of small beaming angles and hence one-dimensional propaga-

tion (e.g., Genzel 1986; Nedoluha & Watson 1991). To perform the numerical integrations, a choice must be made for the product of the brightness temperature T_b of the continuum radiation that is incident onto the masing region and the solid angle of the maser beam [note $T_b = 4\pi^3 c^2 I(\omega)/k\omega^2$]. All of the results presented here are based on an incident $T_b \Delta\Omega = 0.1$ K sr. We have verified that our results are insensitive to this choice by performing additional computations in which the incident $T_b \Delta\Omega$ is varied over several orders of magnitude. We consider only incident radiation that is unpolarized. All of the intensities obtained by solving equations (2) and (8)–(10) are proportional to the choice for the decay rate Γ , or $(\Gamma + \Gamma_v)$ when cross-relaxation is included according to § 2.2. In presenting actual intensities or brightness temperatures, we adopt $\Gamma = 1$ s⁻¹, which is representative of the more realistic choice $(\Gamma + \Gamma_v) = 1$ s⁻¹ (see §§ 2.2 and 4). The results that we present for $T_b \Delta\Omega > 10^{11}$ K sr may be unreliable for $\theta \neq 0$. For $T_b \Delta\Omega = 10^{11}$ K sr, the characteristic rate for stimulated emission

$$R \simeq AkT_b \Delta\Omega / 4\pi\hbar\omega \quad (31)$$

is about 10 s⁻¹, whereas the values of $g\Omega$ in the stronger two hyperfine transitions are about 100 s⁻¹ for magnetic fields of 10 mG.

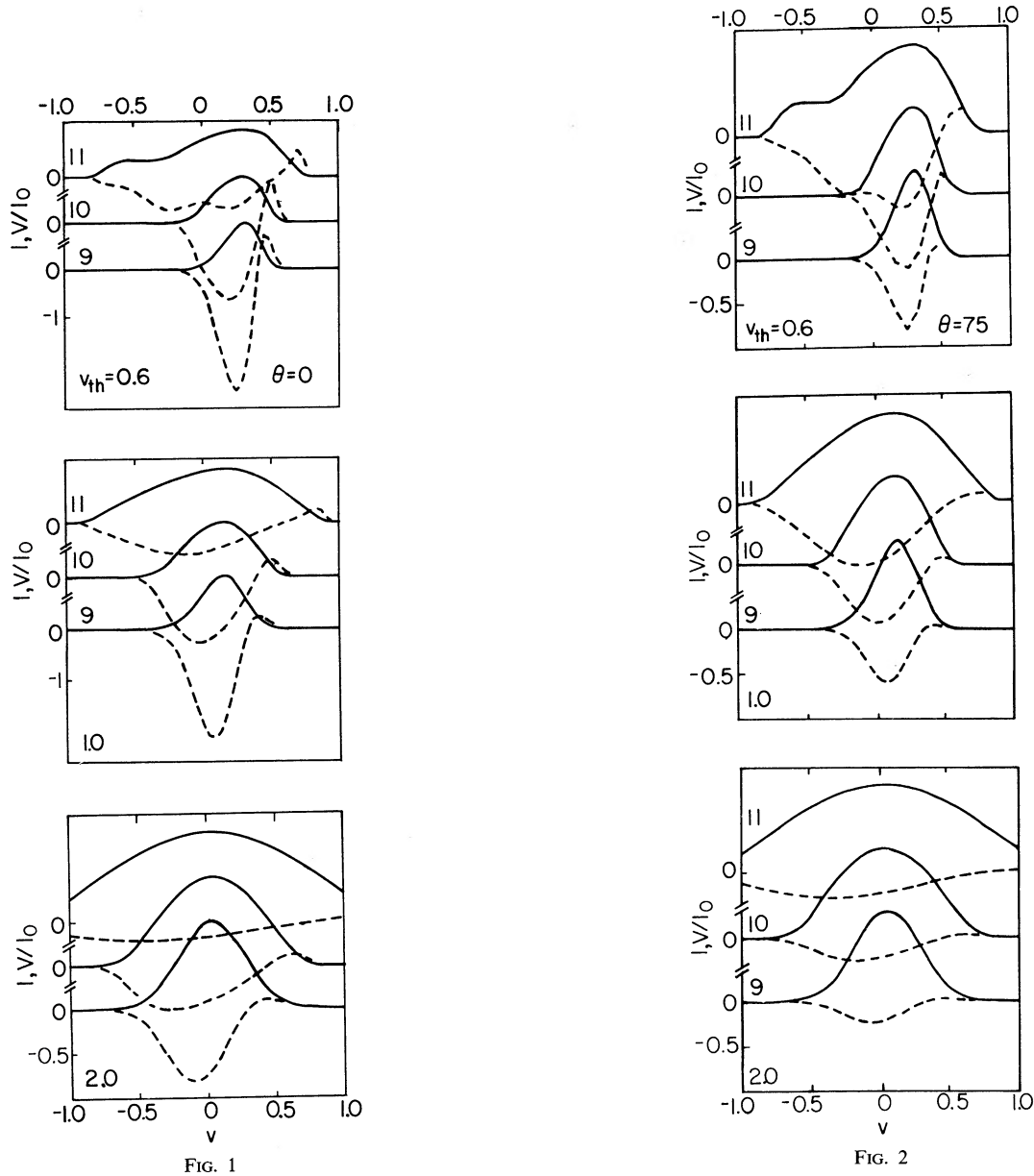


FIG. 1.—Intensity I (solid line) and fractional circular polarization (dashed line) given as the ratio of the Stokes V parameter to the peak value of the intensity I_0 , for the 22 GHz maser transition. I and (V/I_0) are presented as a function of frequency (expressed as the equivalent Doppler velocity in km s⁻¹) across the spectral line. All intensities I are normalized to the same peak height; (V/I_0) are in units of 10^{-3} ($B/20$ mG) as indicated. The three panels are obtained at three thermal velocities v_{th} (km s⁻¹) as indicated. Within each panel, spectra are presented at three radiative fluxes (peak values) $T_b \Delta\Omega$ (K sr) = 0.5×10^9 , 0.5×10^{10} , 0.5×10^{11} , and are labeled by the exponents 9, 10 and 11. The propagation angle is $\theta = 0$ for all spectra ($v = 0$ at the rest frequency for the 6–5 transition).

FIG. 2.—Same as Fig. 1 except that here the propagation angle $\theta = 75^\circ$

Hence, the requirement $g\Omega \gg R$ for ignoring the off-diagonal elements of the density matrix in our calculations is not well satisfied at higher values for $T_b \Delta\Omega$ and all magnetic fields within the range of chief interest ($B \lesssim 10$ mG). At $\theta = 0$, the off-diagonal elements that become significant with increasing intensity are not present. Our results at $\theta = 0$ should thus be reliable up to the highest $T_b \Delta\Omega$ for which they are presented.

In Figures 1–4, we present spectral line profiles of the total intensity and of the fractional circular and linear polarization for representative choices of the relevant parameters—the propagation angle θ and the thermal breadth v_{th} (FWHM) of the Maxwellian distribution of particle velocities. For a kinetic temperature T in kelvins, $v_{th} = 0.5 (T/100)^{1/2}$ km s⁻¹. Line profiles are presented for peak maser fluxes $T_b \Delta\Omega$ of 0.5×10^9 , 0.5×10^{10} , and 0.5×10^{11} K sr. The profiles at the lowest flux are representative of those of the lower fluxes before the rebroadening of the spectral line occurs (see Fig. 5; also Nedoluha & Watson 1991). The profiles at the other two fluxes are representative for intermediate and nearly complete rebroadening of the spectral line. Narrowing occurs because the amplification is greatest near line center when the molecules have a Maxwellian velocity distribution. Rebroadening occurs when the velocity distribution deviates from a Maxwellian due to rapid stimulated emission and the populations at velocities corresponding to line center are depleted. Except for Figure 9, all of our calculations are performed for a magnetic field strength $B = 20$ mG. In the calculations of this section, Stokes V is proportional to B at least up to the highest magnetic fields (80 mG) studied in Figure 9. We emphasize that as a result of the narrowing and rebroadening of the spectral lines of masers as a function of the emergent radiative flux, there is a relationship between the flux (and hence the polarization characteristics) and the spectral line breadth (Nedoluha & Watson 1991). For example, observed spectral line breadths Δv less than about 0.8 km s⁻¹ (FWHM) are only compatible with fluxes $T_b \Delta\Omega \gtrsim 10^{10}$ K sr. Without additional causes for broadening, larger observed breadths require larger values for $T_b \Delta\Omega$. Our calculations for the 22 GHz maser transition do, of course, include all three hyperfine

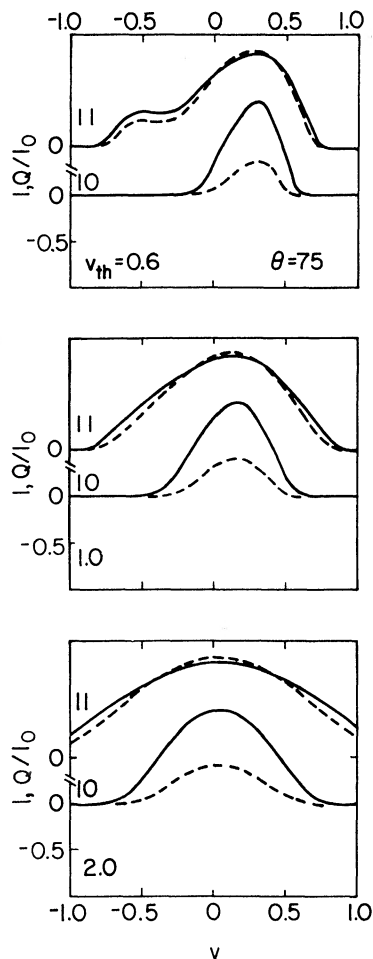


FIG. 3

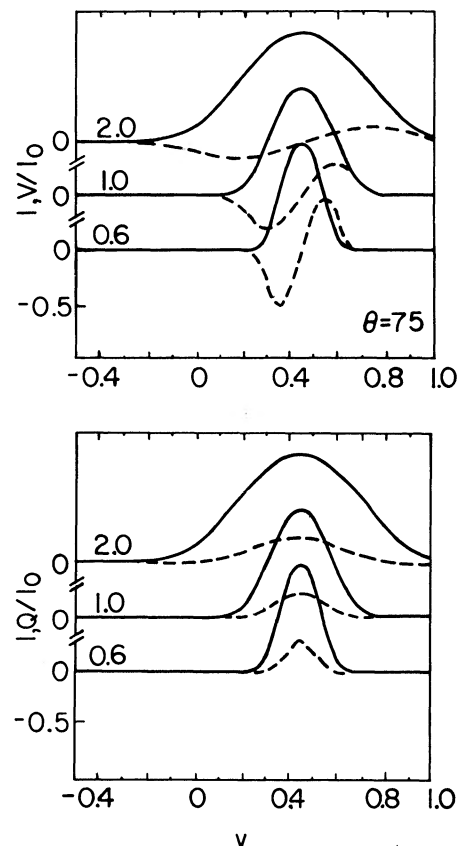


FIG. 4

FIG. 3.—Similar to Fig. 1 except that here the fractional linear polarization (the ratio of the Stokes Q parameter to the peak value of the intensity I_0) is given (dashed line), together with the normalized intensity I (solid line). (Q/I_0) is in units of 0.1. The propagation angle is $\theta = 75^\circ$, and spectra are shown for only two radiative fluxes (Q/I_0 is negligible at $T_b \Delta\Omega = 0.5 \times 10^9$ K sr).

FIG. 4.—Similar to Fig. 1 except that here only the hyperfine 7–6 transition is included in the calculations. Normalized I (solid line) and V/I_0 in units of $10^{-3} [B/20 \text{ mG}]$ (dashed line) are shown in the upper panel. Normalized I and Q/I_0 in units of 0.1 (dashed line) are in the lower panel. All profiles are for a peak flux $T_b \Delta\Omega = 0.5 \times 10^{10}$ K sr. The three profiles are calculated with different v_{th} (km s⁻¹) according to the labels. The location of $v = 0$ is still at the rest frequency of the hyperfine 6–5 transition, and the propagation angle θ is 75° .

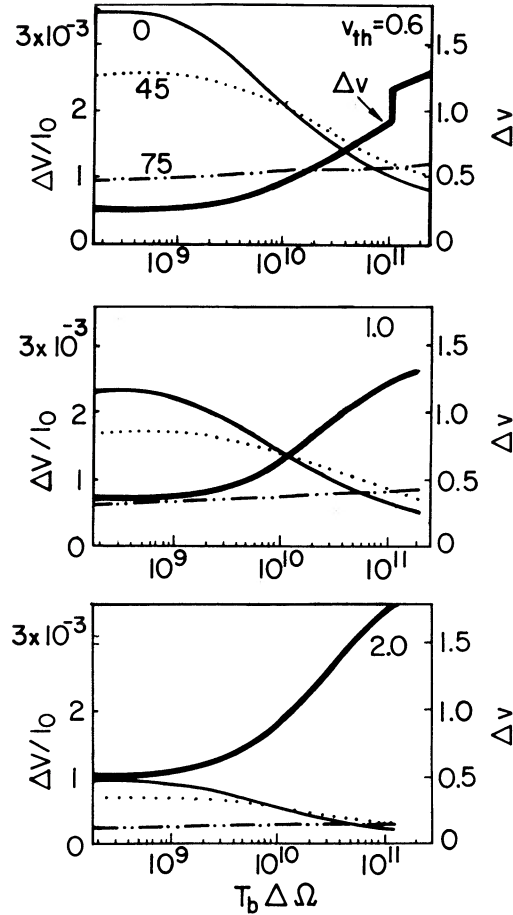


FIG. 5.—Fractional circular polarization difference $(V_{\max} - V_{\min})/I_0 = \Delta V/I_0$ (in units of $10^{-3} [B/20 \text{ mG}]$) and spectral line breadth $\Delta v \text{ km s}^{-1}$ (FWHM) vs. peak emergent maser flux $T_b \Delta \Omega \text{ K sr}$. Each panel represents calculations at a particular choice of $v_{\text{th}} \text{ km s}^{-1}$ as indicated. The three curves for $\Delta V/I_0$ in the upper panel are labeled according to the propagation angle θ ; those in the lower panel have the same meaning. The discontinuity in Δv for the $v_{\text{th}} = 0.6 \text{ km s}^{-1}$ profile occurs because the peak of the hyperfine 5–4 transition becomes equal to one-half of the peak of the total I profile at this $T_b \Delta \Omega$.

components as described in § 2.1. For comparison purposes, we also present results from calculations involving the hyperfine 7–6 transition alone.

The profiles for the circular polarization V of the 22 GHz transition are quite different from that of a single spectral line. In all cases, the overlap of hyperfine components causes one of the circular polarizations to dominate across most of the spectral line. We have examined numerous additional profiles of V at higher, lower, and intermediate values for $T_b \Delta \Omega$. Only at the lowest kinetic temperature ($v_{\text{th}} = 0.5 \text{ km s}^{-1}$) and for much lower $T_b \Delta \Omega$ do we find profiles for V that are approximately antisymmetric about line center. The spectral breadths for these ($\Delta v \simeq 1/4 \text{ km s}^{-1}$) would be smaller than what is observed and a kinetic temperature would be required that is lower than seems to be required from considerations of the pumping. For comparison, we artificially suppress the other two hyperfine transitions and calculate profiles for V for the hyperfine 7–6 transition alone. These do exhibit the expected antisymmetric variation about the center of the spectral line as shown in Figure 4.

To understand why one circular polarization tends to dominate, consider the equations of radiative transfer in the unsaturated ($R \ll \Gamma$) regime. Here, the populations and hence C_{ω}^{FF} and A_{ω}^{FF} are independent of intensity. Integration of equation (10) yields

$$V(\omega)/I(\omega) = (C_{\omega}^{76} + C_{\omega}^{65} + C_{\omega}^{54}) s, \quad (32)$$

where s is the length of the path through the masing region. Thus, the sense of the net circular polarization as a function of frequency is given by the sign of $(C_{\omega}^{76} + C_{\omega}^{65} + C_{\omega}^{54})$. In the unsaturated limit where all of the $[n(F, a, v) - n(F, b, v)]$ are equal and independent of flux, and their dependence on velocity is that of a Maxwellian, equation (13) as well as equations (11) and (12), can then readily be evaluated to give a quantity proportional to the sum on the right-hand side of equation (32),

$$(C_{\omega}^{76} + C_{\omega}^{65} + C_{\omega}^{54}) \propto [(v - 0.45) \exp \{ -[(v - 0.45)/(0.6v_{\text{th}})]^2 \} + 0.52v \exp \{ -[v/0.6v_{\text{th}}]^2 \} + 0.052(v + 0.58) \exp \{ -[(v + 0.58)/(0.6v_{\text{th}})]^2 \}] B \cos \theta. \quad (33)$$

As in the figures, we express the frequency of the radiation in equation (33) in terms of the equivalent Doppler velocity (km s^{-1}),

$$v = (\omega - \omega^{65})c/\omega^{65} \quad (34)$$

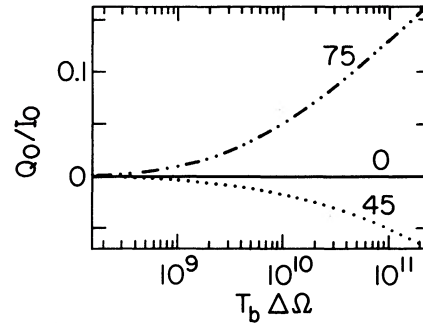


FIG. 6.—Fractional linear polarization (Q_0/I_0) at the peak of the intensity I (also the peak in Q) vs. peak maser flux $T_b \Delta\Omega$ K sr. To the accuracy that can be shown, these curves are the same for the full 22 GHz profile and for the hyperfine 7–6 transition alone. They are also the same for the three values of v_{th} (0.6, 1.0, and 2.0 km s $^{-1}$) that we consider.

relative to the angular frequency ω^{65} of the hyperfine 6–5 transition at rest and in the absence of a magnetic field. Equation (33) passes through zero at $v = 0.38, 0.31,$ and 0.28 km s $^{-1}$ for $v_{th} = 0.6, 1.0,$ and 2.0 km s $^{-1}$, respectively. The locations of these zeros in equation (33) and hence in the Stokes V parameter are in excellent agreement with those found for the profiles before rebroadening in Figures 1 and 2. They indicate an asymmetric $V(\omega)$ since these zeros are well away from the peaks in the total intensities. The locations of these peaks in the intensities in the unsaturated regime could also be verified by a calculation for the $A_{\omega}^{FF'}$ analogous to that leading to equation (33). Under certain circumstances, the profile for V can be related to the derivative of the profile for the intensity I . That is not the case here because of the combined effect of the blending of the three hyperfine components and of having different values of $g\Omega$ for the various states.

When R from equation (31) becomes comparable with Γ , the populations of the magnetic substates of a given hyperfine state are no longer equal. Then, from equation (12), $B_{\omega}^{FF'} \neq 0$ and linear polarization Q is generated. In Figure 6, we show the ratio (Q_0/I_0) at the frequency of the peak in intensity I . As shown in Figures 3 and 4, the variation of $Q(\omega)$ across the spectral line tends to follow the variation in $I(\omega)$. The fractional linear polarization as presented in Figure 6 is essentially the same for all three choices of v_{th} , for the 7–6 transition alone, and for the entire 22 GHz feature with the three hyperfine components. Note that Q is defined here as the difference between the intensities of the radiation polarized perpendicular and parallel to the plane containing the direction of the magnetic field and the line of sight (i.e., $Q = I_{\perp} - I_{\parallel}$).

The Stokes component U of the linear polarization is zero here because the calculations are being performed in the regime $g\Omega \gg R$.

To examine how well the relationship of equation (1) applies to the results of our calculations, we present $(\Delta V \Delta v/I_0)B \cos \theta$ in Figure 7 for representative choices for the propagation angle θ and the thermal breadth v_{th} . For comparison purposes, calculations are also presented for the 7–6 hyperfine transition alone by suppressing the other two hyperfine components.

Although equation (1) was obtained for the completely antisymmetric profile for V due to a single line, we see that it is still an excellent way to summarize our calculations at fluxes below those at which significant rebroadening occurs ($T_b \Delta\Omega \approx 10^{10}$ K sr) provided that $\Delta V = (V_{max} - V_{min})$ is taken from the asymmetric profile of V that we calculate. Our “best value” for the constant \mathcal{A} in equation (1) is 0.020 km s $^{-1}$ G $^{-1}$ based on the $\theta = 0$ curve at $T_b \Delta\Omega = 10^9$ K sr for $v_{th} = 1.0$ km s $^{-1}$ (400 K) in Figure 7. The value of \mathcal{A} from the 7–6 transition alone in Figure 7 is 0.015 km s $^{-1}$ G $^{-1}$ which is almost exactly the same as the 0.013 km s $^{-1}$ G $^{-1}$ obtained by FG for the 7–6 transition. In the regime $T_b \Delta\Omega \gtrsim 10^{10}$ K sr, deviations from equation (1) with $\mathcal{A} = 0.020$ km s $^{-1}$ G $^{-1}$ range over less than a factor of about 2. In practice, they may be smaller. The lower v_{th} can probably be eliminated from considerations about the pumping of the masers (e.g., Neufeld & Melnick 1990). It also seems unrealistic to expect that there can be

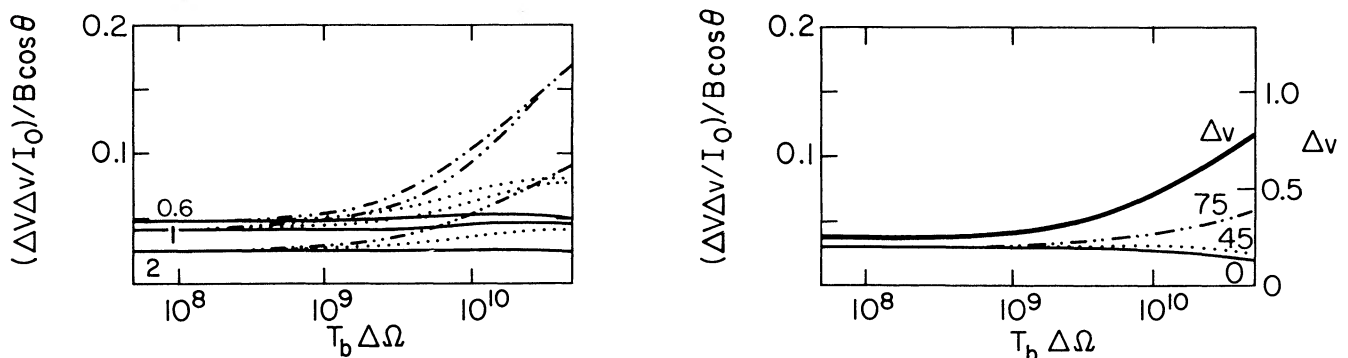


FIG. 7.—The fractional circular polarization as described by the quantity $(\Delta V \Delta v/I_0)B \cos \theta$ [km s $^{-1}$ G $^{-1}$] vs. peak maser flux $T_b \Delta\Omega$ K sr. *Left panel*: full 22 GHz transition; *right panel*: hyperfine 7–6 transition alone (in the right panel, the spectral line breadth Δv is also shown). Calculations are shown for three propagation angles θ (0° , 45° , and 75°) which are identified by the type of line as labeled in the right panel. In the left panel, calculations are shown for three values of v_{th} (0.6, 1.0, and 2.0 km s $^{-1}$) as indicated at low $T_b \Delta\Omega$ where the calculations for different θ merge. In the right panel, calculations for all three v_{th} yield the same results.

enough gas at temperatures near 1000 K in interstellar clouds so that a large fraction of the 22 GHz masers can have v_{th} as large as 2 km s^{-1} . At fluxes above 10^{10} K sr , the deviations between equation (1) and the range of possibilities reflected in our calculations become larger—especially at propagation angles $\theta \lesssim 45^\circ$ and perhaps as large as factor of 5 at 10^{11} K sr . If the propagation angles θ are not too large ($\theta \gtrsim 45^\circ$), our calculations agree with equation (1) to a factor of about two at all fluxes with $\mathcal{A} = 0.02 \text{ km s}^{-1} \text{ G}^{-1}$.

The basis for equation (1) is, of course, that $(\Delta V \Delta v / I_0)$ is constant in the unsaturated regime as the spectral line of the maser becomes narrower and more intense. We can see this readily, at least for the case of a single transition. Using the fact that the optical depths of interest are much greater than one and that the variation of the optical depth τ_ν as a function of the frequency (expressed as a Doppler velocity ν) across the spectral line is a Maxwellian, we can find the spectral line breadth

$$\Delta \nu / v_{\text{th}} \simeq \tau_0^{-1/2}. \quad (35)$$

Here, τ_0 is the optical depth at the peak of the intensity.

To find the maximum in the Stokes V parameter across the spectral line, differentiate the V obtained from equation (32). Use the fact that C_ω for a single transition in the unsaturated regime is proportional to ν multiplied by a Maxwellian and that τ_ν is proportional to this Maxwellian. The maximum in V occurs at a velocity ν_m which is then given by the solution of

$$\tau_0 \exp [-(\nu_m/0.6v_{\text{th}})^2] = \frac{1 - 2(\nu_m/0.6v_{\text{th}})^2}{2(\nu_m/0.6v_{\text{th}})^2}. \quad (36)$$

Since $(\nu_m/0.6v_{\text{th}})^2 \ll 1$,

$$(\nu_m/0.6v_{\text{th}})^2 \simeq 1/(2\tau_0). \quad (37)$$

Inserting this back into equation (32) and relating I_ν to I_0 yields

$$\Delta V / I_0 \propto (\tau_0)^{1/2}. \quad (38)$$

The product of equations (35) and (38) is thus constant with increasing maser flux as long as the maser is unsaturated. It is the basis for understanding the valuable relationship of equation (1).

In Figure 8, we show directly the relationship between $\Delta V / I_0$ and the spectral line breadth $\Delta \nu$, for representative thermal breadths and propagation angles. The peak linear polarization Q_0 / I_0 is also shown. The curves in Figure 8 for $\Delta V / I_0$ are mostly at maser fluxes where at least some rebroadening is indicated in Figures 5 and 6. Variations in both $\Delta V / I_0$ and in $\Delta \nu$ are small before rebroadening occurs. These larger portions of the curves in Figures 5 and 6 are thus compressed into the “hooks” at the low $\Delta \nu$ ends of the curves. The Q_0 / I_0 given here represent only the region after rebroadening has begun since $Q = 0$ at lower fluxes. For increasing v_{th} , the polarization properties of the 22 GHz hyperfine transitions tend to behave more like that of a single transition.

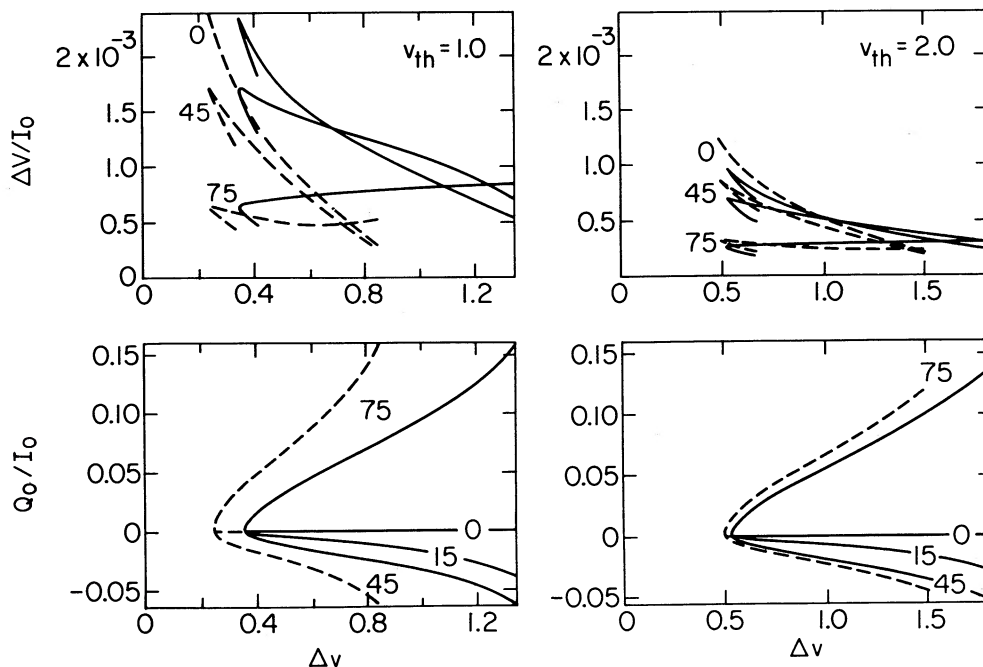


FIG. 8.—Fractional circular polarization differences $(\Delta V / I_0)(B/20 \text{ mG})$ (upper panels) and fractional linear polarizations (Q_0 / I_0) at peak intensity (lower panels) vs. spectral line breadth $\Delta \nu$ (FWHM) in km s^{-1} . The panels on the left-hand side are calculated with $v_{\text{th}} = 1.0 \text{ km s}^{-1}$ and those on the right-hand side, with $v_{\text{th}} = 2.0 \text{ km s}^{-1}$. Solid lines: full 22 GHz spectral line; dashed lines: only the hyperfine 7-6 transition. Calculations are performed for propagation angles θ (0° , 15° , 45° , and 75°) as indicated. Note that the ends of the curves at small $\Delta \nu$ represent the beginnings of the rebroadening of the spectral lines. Except for the short hooks in the upper panels, all of the results represent profiles that are at least partly rebroadened.

For most observed line breadths, Q_0/I_0 should be small (less than $\sim 10\%$), in general agreement with observation. A comparison of this linear polarization with that found for transitions involving states of low angular momentum in the regime where $g\Omega \gg R$ and Γ (e.g., Western & Watson 1984; Nedoluha & Watson 1990a) provides an indication of the decrease in linear polarization with increasing angular momentum. As suggested previously, the 3–2 transition is representative of transitions involving states of higher angular momenta. Although a full treatment of the hyperfine states was included in the only previous calculation of the linear polarization of the 22 GHz transition (Deguchi & Watson 1986), this earlier calculation used the Sobolev approximation for the radiative transfer of the maser radiation. This approximation probably overestimates the fractional polarization at the lower radiative fluxes.

Because the circular polarization in the regime here is proportional to the magnetic field strength B , the calculations presented in the foregoing figures have all been computed using a single strength for the magnetic field $B = 20$ mG. To show explicitly that V is proportional to B , we give $\Delta V/I_0$ in Figure 9 for a series of values for B and as a function of Δv . If the contribution of $Q(\omega)$ in the rate equations (2) were significant, for example, $\Delta V/I_0$ would not be expected to be proportional to B . Although the $\Delta V/I_0$ in Figure 9 are proportional to B , they are not proportional to $\cos \theta$ as is the case at fluxes below that at which rebroadening occurs (see also Figs. 4 and 5). The additional dependence on θ occurs because the populations of the magnetic substates become unequal in a manner that depends upon θ .

4. DISCUSSION

It seems difficult to avoid the result that the spectrum of the circular polarization V is quite asymmetric, with the net polarization of one sense being larger than the other by a factor of 2–3 or more. Previous calculations have also shown that the 22 GHz transition should be a blend of the strongest hyperfine components except possibly at kinetic temperatures below 100 K (Nedoluha & Watson 1991). Such low temperatures seem unlikely since they apparently do not allow sufficient pumping for the maser which seems to require temperatures of about 400 K (e.g., Neufeld & Melnick 1990). In addition, the calculated spectral line breadths, Δv ($\approx 1/4$ km s $^{-1}$) at temperatures below 100 K, would be significantly smaller than the observed breadths. The smooth and symmetrical line profiles tend to indicate that there is little, if any, additional breadth of the spectral lines due to emission from a number of separate components with $\Delta v \approx 1/4$ km s $^{-1}$. Even if there were, it is not evident that the antisymmetric profiles of V similar to those due to a single transition would result. Some form of turbulence probably does contribute to the breadths of spectral lines due to nonmasing transitions at radio frequencies from the interstellar gas, but the relevant length scales for the formation of these spectral lines is several orders of magnitude greater than the sizes of the 22 GHz masers ($\approx 10^{13}$ cm). Selective pumping of one of the hyperfine components also is difficult to imagine. The spectral line breadths of the radiative transitions at infrared wavelengths that are involved in the pumping are much greater than the hyperfine splittings, and these transitions are expected to have large optical depths (typically 10^2 – 10^3) under conditions in which the pumping is adequate. Selectivity is also unlikely because there are a number of pathways that contribute to populating the masing states.

The observational technique used by FG to calibrate the instrumental gains of the right and left circular modes is similar to that described by Crutcher & Kazes (1983). In this, it is *assumed* in the analysis that the power in the left and right circularly polarized line profiles is the same. Hence, the resulting profiles of the Stokes V parameter automatically have zero integrated area and tend to appear antisymmetric, as is characteristic of V for a single transition. We thus believe that our asymmetric profiles of V are compatible with the currently available observational information about the 22 GHz masers. Although the observations may not provide reliable information about the profile of V , the difference $\Delta V = (V_{\max} - V_{\min})$ apparently is insensitive to such uncertainties in calibration. Fortunately, we have found that this is the relevant quantity to relate the strength of the magnetic field to the observational data.

The rates at which the molecular velocities relax toward a Maxwellian distribution and the population of the magnetic substates of an energy level relax toward equality are expected to be much larger than the rate Γ at which the inverted population of the maser decays. Trapping of infrared radiation is the dominant cause for both types of relaxation. The rates probably are slightly different

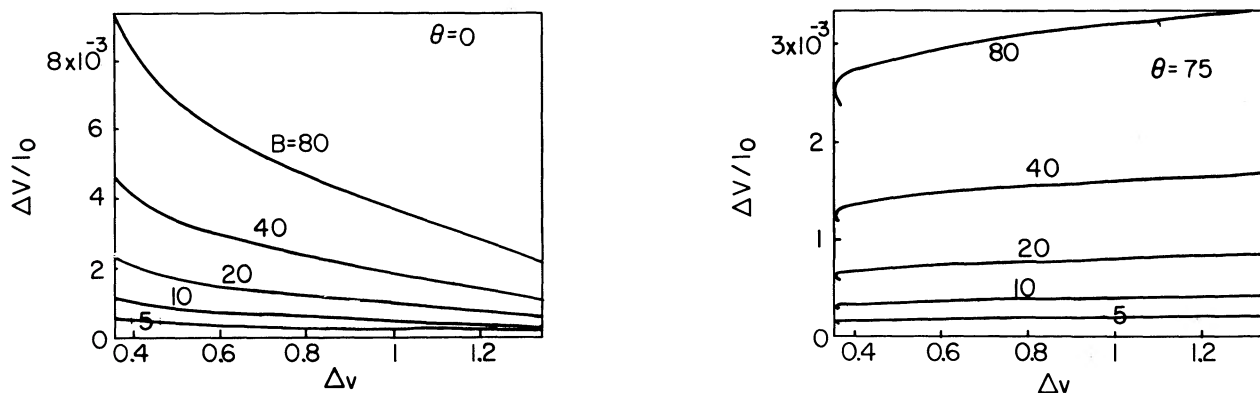


FIG. 9.—Fractional circular polarization difference ($\Delta V/I_0$) for several values of the magnetic field strength B in mG as a function of spectral line breadth Δv . Results of calculations are shown for two propagation angles θ (0° , left panel; 75° , right panel). Except for the hooks in the lower panel, rebroadening of the spectral profiles has begun in all of these calculations. These calculations demonstrate that $(\Delta V/I_0)$ is proportional to B for the relevant range of strengths for the magnetic field.

though we ignore this and designate the rate for both as Γ_v —the rate for cross-relaxation. The rate Γ_v is insensitive to the details of the model for 22 GHz masers and is determined roughly by only the Einstein A -coefficients for infrared, radiative transitions that involve the maser states. It is $\Gamma_v \simeq 2 \text{ s}^{-1}$ at 400 K based on recent detailed calculations (Anderson & Watson 1991). This rate is in excellent agreement with the estimate of Goldreich & Kwan (1974).

The maser flux $T_b \Delta\Omega$ at which both the spectral line profile and the polarization properties of the maser radiation change from those of the low-intensity regime is determined by the stimulated emission rate R for which $R = (\Gamma + \Gamma_v) \simeq \Gamma_v$. Rebroadening of the line profile and the changes in polarization properties have a related origin. When $R \lesssim \Gamma_v$, the maser radiation influences the populations. It causes the velocity dependence of the molecular excitation to deviate from a Maxwellian and the populations of the magnetic substates of an energy level to become unequal. For a reasonable approximation for the effect of cross-relaxation in determining the molecular populations, we show that the spectral and polarization characteristics are determined exactly by the ratio $T_b \Delta\Omega / (\Gamma + \Gamma_v)$. In practice, we do not have reliable information about $T_b \Delta\Omega$ since the beaming angle $\Delta\Omega$ is essentially unknown from direct observation and may range over several orders of magnitude. We thus use the observations of the spectral line breadth in place constraints on $T_b \Delta\Omega / (\Gamma + \Gamma_v)$ and hence on the polarization characteristics. The analysis does not thus depend upon specific values for Γ and Γ_v , or even upon the premise that cross-relaxation is important.

There is one sense in which the approximate magnitude of $(\Gamma + \Gamma_v)$ is important for our analysis. Our calculations are performed in the limit in which off-diagonal elements of the quantum mechanical density matrix can be ignored. This requires $g\Omega \gg R$. Many, if not most, line breadths for 22 GHz maser features (including the sample of FG) that seem to be individual components are smaller than about 1 km s^{-1} (FWHM). The relevant magnetic fields seem to be greater than at least a few mG. Magnetic fields at least this large in regions of star formation are also indicated by the well split, Zeeman features of the OH masers. Thus, $g\Omega$ is greater than R by at least a factor of about 10 for the $F = 7-6$ and $6-5$ hyperfine transitions which make the main contributions to Stokes V . Results of detailed calculations which do include off-diagonal elements of the density matrix suggest that the $g\Omega \gg R$ limit is then adequate (Nedoluha & Watson 1990b), though barely so when the difference is only one factor of 10. The $g\Omega \gg R$ approximation may also be valid for those masers with $\Delta v \lesssim 1 \text{ km s}^{-1}$ as well if their additional line breadth is due to causes other than rebroadening. The fractional linear polarization of the 22 GHz maser radiation also tends to be low ($Q_0/I_0 \lesssim 0.1$) and is thus consistent with R that is not much greater than 1 s^{-1} for most 22 GHz masers. The high linear polarizations of the maser flares in Orion and in W75S are notable exceptions. We believe that this polarization probably is due to anisotropic pumping. The result from line breadth considerations that the maser radiation from the flares in Orion and W49 is highly beamed (Nedoluha & Watson 1991) would seem to make the notion of anisotropic pumping more plausible. This allows the optical depths to be smaller in directions other than that along the direction of propagation of the maser radiation. Anisotropic pumping for masing in the presence of a magnetic field has been treated elsewhere (Western & Watson 1983, 1984; Nedoluha & Watson 1990a).

In summary, we find that the measurement of the circular polarization of 22 GHz water masers can be a surprisingly reliable indicator of $B \cos \theta$ despite the complicating aspects of the radiative transfer that are treated here. The order-of-magnitude uncertainty that previously seemed to be inherent due to lack of knowledge about which hyperfine component is masing has been eliminated. The relative importance of the various hyperfine components is determined by the radiative transfer and the inferred magnetic field strengths are insensitive to uncertainties in the blending of these components. By focusing attention on spectral line profiles with $\Delta v \gtrsim 0.8 \text{ km s}^{-1}$, the simple relationship of equation (1) with $\mathcal{A} = 0.020 \text{ km s}^{-1} \text{ G}^{-1}$ can be applied to infer $B \cos \theta$ with reasonable confidence that the complications studied here cause an uncertainty that is less than about a factor of 2. If there is reason to believe that $\theta \gtrsim 45^\circ$ the uncertainty is significantly reduced. Some caution may still be warranted because we have not yet performed complete calculations for the full range of parameters that describe effects of the type treated by Nedoluha & Watson (1990b).

We are especially indebted to R. M. Crutcher for a number of discussions about the observations, and to D. Fiebig and R. Gusten for verifying that our asymmetric profiles for V are compatible with their data. We are also grateful to J. Moran for helpful comments. This research has been supported by NASA grant NAGW-1104 and NSF grant AST 89-19614. The computations were performed with an allocation from the National Center for Supercomputing Applications at UIUC.

REFERENCES

- Alcock, C., & Ross, R. R. 1985, *ApJ*, 290, 433
 Anderson, N., & Watson, W. D. 1991, paper presented at the 177th meeting of the American Astronomical Society
 Crutcher, R. M., & Kazes, H. 1983, *A&A*, 125, L23
 Deguchi, S., & Watson, W. D. 1986, *ApJ*, 302, 750
 ———. 1990, *ApJ*, 354, 649
 Fiebig, D., & Güsten, R. 1989, *A&A*, 214, 333 (FG)
 Genzel, R. 1986, in *Masers, Molecules, and Mass Outflows in Star-Forming Regions*, ed. A. D. Haschick (Westford, MA: Haystack Observatory), 233
 Goldreich, P., Keeley, D. A., & Kwan, J. Y. 1973, *ApJ*, 182, 55
 Goldreich, P., & Kwan, J. Y. 1974, *ApJ*, 190, 27
 Gordy, W., & Cook, R. L. 1970, *Microwave Molecular Spectra* (New York: Wiley Interscience)
 Kukolich, S. 1969, *J. Chem. Phys.*, 50, 3751
 Litvak, M. M. 1970, *Phys. Rev. A*, 2, 2107
 Messiah, A. 1962, *Quantum Mechanics* (Amsterdam: North-Holland)
 Nedoluha, G. E., & Watson, W. D. 1988, *ApJ*, 335, L19
 ———. 1990a, *ApJ*, 354, 660
 ———. 1990b, *ApJ*, 361, L53
 ———. 1991, *ApJ*, 367, L63
 Neufeld, D. A., & Melnick, G. J. 1990, *ApJ*, 352, L9
 Reid, M. J., & Moran, J. M. 1981, *ARA&A*, 19, 231
 Townes, C. H., & Schawlow, A. L. 1975, *Microwave Spectroscopy* (New York: Dover)
 Western, L. R., & Watson, W. D. 1983, *ApJ*, 275, 195
 ———. 1984, *ApJ*, 285, 158